
CAE: Repurposing the Critic as an Explorer in Deep Reinforcement Learning

Yexin Li¹ Pring Wong¹ Hanfang Zhang² Shuo Chen¹ Siyuan Qi³

Abstract

Exploration remains a critical challenge in reinforcement learning, as many existing methods either lack theoretical guarantees or fall short of practical effectiveness. In this paper, we introduce CAE, a lightweight algorithm that repurposes the value networks in standard deep RL algorithms to drive exploration without introducing additional parameters. CAE utilizes any linear multi-armed bandit technique and incorporates an appropriate scaling strategy, enabling efficient exploration with provable sub-linear regret bounds and practical stability. Notably, it is simple to implement, requiring only around 10 lines of code. In complex tasks where learning an effective value network proves challenging, we propose CAE+, an extension of CAE that incorporates an auxiliary network. This extension increases the parameter count by less than 1% while maintaining implementation simplicity, adding only about 10 additional lines of code. Experiments on MuJoCo and MiniHack show that both CAE and CAE+ outperform state-of-the-art baselines, bridging the gap between theoretical rigor and practical efficiency.

1. Introduction

Exploration in reinforcement learning (RL) remains a fundamental challenge, particularly in environments with complex dynamics or sparse rewards. Although algorithms such as DQN (Mnih et al., 2015), PPO (Schulman et al., 2017), SAC (Haarnoja et al., 2018), DDPG (Lillicrap et al., 2016), TD3 (Fujimoto et al., 2018), IMPALA (Espeholt et al., 2018), and DSAC (Duan et al., 2021; 2023) have demonstrated impressive performance on tasks like Atari games (Mnih et al., 2013; 2015), StarCraft (Vinyals et al., 2019), Go (Silver et al., 2017), *etc.*, they often depend on rudimentary exploration strategies. Common approaches, such as ϵ -greedy or injecting noise into actions, are typically inefficient and

struggle in scenarios with delayed or sparse rewards.

For decades, exploration with proven optimality in tabular settings has been available (Kearns & Singh, 2002). More recently, methods with provable regret bounds have been developed for scenarios involving function approximation, including linear functions (Osband et al., 2016; 2019; Jin et al., 2018; 2020; Agarwal et al., 2020), kernels (Yang et al., 2020), and neural networks (Yang et al., 2020). However, while linear and kernel-based approaches make strong assumptions about the RL functions, provable methods based on neural networks suffer from prohibitive computational costs, specifically $O(n^3)$, where n is the number of parameters in the RL network. Moreover, some studies (Ash et al., 2022; Ishfaq et al., 2024a) propose algorithms with theoretical guarantees under the linearity assumption and attempt to extend them directly to deep RL settings without further proof. Other works (Ishfaq et al., 2021; 2024b) provide provable bounds for deep RL, but they are either practically burdensome or rely on an unknown sampling error.

A more practical approach to exploration relies on heuristics, leading to the development of several empirically successful methods, including Pseudocount (Bellemare et al., 2016), ICM (Pathak et al., 2017), RND (Burda et al., 2019b), RIDE (Raileanu & Rocktäschel, 2020), NovelD (Zhang et al., 2021a), AGAC (Flet-Berliac et al., 2021), and E3B (Henaff et al., 2022; 2023). These methods typically use internally generated bonuses to encourage agents to explore novel states based on specific metrics. For example, RND (Burda et al., 2019b) leverages the prediction error of a randomly initialized target network as the exploration bonus, while RIDE (Raileanu & Rocktäschel, 2020) combines errors from forward and inverse dynamics models to compute the bonus. However, these methods introduce bias to the external rewards from the environment, lack theoretical guarantees, and are primarily guided by intuitive heuristics. Additionally, they often require training extra networks beyond the standard value or policy networks used in deep RL algorithms, resulting in increased computational overhead.

In this work, we aim to combine the strengths of both theoretically grounded and empirically effective exploration methods. Provably efficient exploration methods are fundamentally rooted in the theory of Multi-Armed Bandits (MAB) (Li et al., 2010; Chu et al., 2011; Agrawal & Goyal,

¹State Key Laboratory of General Artificial Intelligence, BIGAI, Beijing, China ²Shandong University ³Gyges Labs. Correspondence to: Yexin Li <liyexin@bigai.ai>.

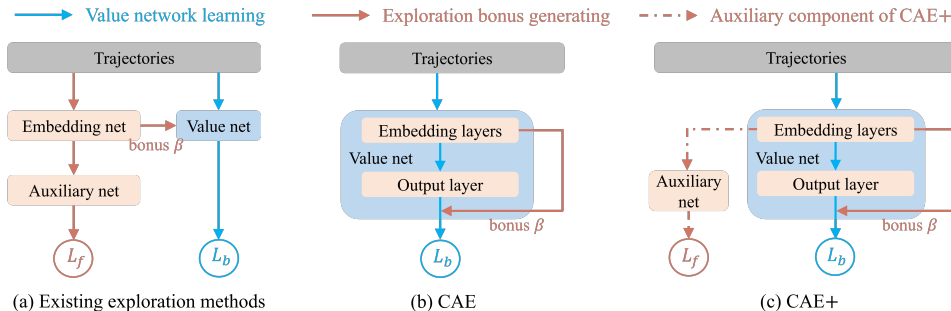


Figure 1. Comparison of existing exploration methods, such as E3B (Henaff et al., 2022), with CAE and CAE+. Here, L_b represents the Bellman loss used to update the state- or action-value function, while L_f refers to the loss of the auxiliary network. E3B requires additional networks to generate exploration bonuses, while CAE utilizes the embedding layers of the value network for bonuses, resulting in reduced computational overhead and no additional parameters. CAE+ extends CAE by incorporating a small auxiliary network to enhance performance in sparse reward environments, with only a minor increase in parameters.

2013; Wen et al., 2015; Zhang et al., 2021b; Zhou et al., 2020). Building on this foundation, we hypothesize that advanced techniques from **neural MAB** can be effectively adapted for exploration in **deep RL**. Existing studies (Zahavy & Mannor, 2019; Riquelme et al., 2018; Xu et al., 2022) indicate that decoupling deep representation learning from exploration strategies shows promise for achieving efficient exploration in neural MAB.

Motivated by these insights, we propose CAE. Unlike existing methods that train additional embedding networks to generate exploration bonuses, CAE leverages the embedding layers of the value network in the RL algorithm and employs linear MAB techniques to produce exploration bonuses. To ensure the practical stability and functionality of CAE, we adopt an appropriate *scaling strategy* (Welford, 1962; Elsayed et al., 2024) to process the bonuses, as elaborated in Section 3.2. Consequently, CAE introduces no additional parameters beyond those in the original algorithm, showcasing that RL algorithms inherently possess strong exploration capabilities if their learned networks are effectively leveraged. Moreover, CAE is simple to implement, requiring only about 10 lines of code. A comparison between CAE and existing exploration methods is in Figure 1.

For tasks with complex dynamics or sparse rewards, learning an effective value network is challenging, often impeding exploration based on it. Accordingly, we propose an extended version CAE+, as illustrated in Figure 1. CAE+ integrates a *small auxiliary network* to facilitate the learning process. The structure of the auxiliary network is carefully designed to prevent severe coupling between the environment dynamics and returns, thereby further enhancing the practical performance of CAE+. Remarkably, this addition results in less than a 1% increase in parameter count and requires only about 10 additional lines of code.

We evaluated CAE and CAE+ on the MuJoCo and MiniHack benchmarks to assess their effectiveness in both dense

and sparse reward environments. CAE consistently improves the performance of state-of-the-art baselines such as PPO (Schulman et al., 2017), SAC (Haarnoja et al., 2018), TD3 (Fujimoto et al., 2018), and DSAC (Duan et al., 2021; 2023). Additionally, CAE+ demonstrates robust performance, consistently outperforming E3B (Henaff et al., 2022), the current state-of-the-art exploration method for MiniHack, across all evaluated tasks. These results highlight the superior reliability and effectiveness of CAE and CAE+ in diverse RL scenarios.

In summary, we make three key contributions. First, we propose lightweight CAE and CAE+, which enable the use of any linear MAB technique for exploration in **deep RL**. By adopting a *scaling strategy* and carefully designing the *small auxiliary network*, we ensure both practical stability and functionality in environments with dense and sparse rewards. Second, our theoretical analysis demonstrates that any deep RL algorithm with CAE or CAE+ achieves a sub-linear regret bound over episodes. Finally, experiments on MuJoCo and MiniHack validate the effectiveness of CAE and CAE+, showcasing their superior performance.

2. Related Work

Multi-Armed Bandits. MAB algorithms address the exploration-exploitation dilemma by making sequential decisions under uncertainty. LinUCB (Li et al., 2010) assumes a linear relationship between arm contexts and rewards, ensuring a sub-linear regret bound (Chu et al., 2011). To relax the linearity assumption, KernelUCB (Valko et al., 2013; Chowdhury & Gopalan, 2017) and NegUCB (Li et al., 2024) transform contexts into high-dimensional spaces and apply LinUCB to the mapped contexts. Neural-UCB (Zhou et al., 2020) and Neural-TS (Zhang et al., 2021b) leverage neural networks to model the complex relationships between contexts and rewards. However, their computational complexity of $O(n^3)$, where n denotes the number of network

parameters, limits their scalability in real-world applications. Neural-LinTS (Riquelme et al., 2018) and Neural-LinUCB (Xu et al., 2022) mitigate this limitation by effectively decoupling representation learning from exploration methods, improving the practicality of neural MAB algorithms.

Table 1. Comparison of exploration algorithms. **Linearity** indicates if the proof applies to linear RL functions. **NN** specifies if the proof applies to deep RL. **Scale to Deep RL** denotes if the algorithm can be extended to Deep RL. **Practical** assesses whether the algorithm operates efficiently without imposing excessive burdens.

Algorithm	Linearity	NN	Scalable to Deep RL	Practical
LSVI-UCB	✓	✗	✗	✗
NN-UCB	✓	✓	✗	✗
OPT-RLSVI	✓	✗	✗	✗
LSVI-PHE	✓	✓	✓	✗
ACB	✓	✗	✓	✓
LMCDQN	✓	✗	✓	✓
CAE & CAE+	✓	✓	✓	✓

Exploration in RL. Common exploration methods in RL, such as ϵ -greedy and stochastic noise, often are sample inefficient and struggle with sparse rewards. While provably efficient algorithms (Kearns & Singh, 2002; Osband et al., 2016; 2019; Jin et al., 2018; 2020; Agarwal et al., 2020; Cai et al., 2020) exist, they face empirical limitations or are primarily theoretical, lacking applicability in deep RL. Some studies (Ash et al., 2022; Ishfaq et al., 2024a) propose algorithms with theoretical guarantees under linearity assumption and directly extend them to deep RL settings. Other works (Ishfaq et al., 2021; 2024b) offer provable bounds for deep RL, while they are either practically burdensome or rely on an unknown sampling error. A comparative analysis among selected algorithms is in Table 1.

Many empirical methods (Bellemare et al., 2016; Pathak et al., 2017; Burda et al., 2019a; Raileanu & Rocktäschel, 2020; Burda et al., 2019b; Zhang et al., 2021a; Flet-Berliac et al., 2021; Henaff et al., 2022; 2023; Jarrett et al., 2023; Yuan et al., 2023) rely on exploration bonuses that incentivize agents to visit novel states, but these approaches often lack theoretical grounding and require training significantly more parameters. In contrast, CAE and CAE+ utilize MAB techniques for exploration, assisted by embedding layers within the RL value networks, providing empirical benefits with minimal additional parameters. Figure 1 illustrates the differences between existing exploration methods, and CAE, CAE+, while Table 2 summarizes the additional networks and parameters of various exploration methods.

3. Methodology

Unless otherwise specified, bold uppercase symbols denote matrices, while bold lowercase symbols represent vectors. \mathbf{I} refers to an identity matrix. Frobenius norm and l_2 norm are

both denoted by $\|\cdot\|_2$. Mahalanobis norm of vector \mathbf{x} based on matrix \mathbf{A} is $\|\mathbf{x}\|_{\mathbf{A}} = \sqrt{\mathbf{x}^T \mathbf{A} \mathbf{x}}$. For an integer $K > 0$, the set of integers $\{1, 2, \dots, K\}$ is represented by $[K]$.

3.1. Preliminary

An episodic Markov Decision Process is formally defined as a tuple $(\mathcal{S}, \mathcal{A}, H, \mathbb{P}, r)$, where \mathcal{S} denotes the state space and \mathcal{A} is the action space. Integer $H > 0$ indicates the duration of each episode. Functions $\mathbb{P} : \mathcal{S} \times \mathcal{A} \times \mathcal{S} \rightarrow [0, 1]$ and $r : \mathcal{S} \times \mathcal{A} \rightarrow [0, 1]$ are the Markov transition and reward functions, respectively. During an episode, the agent follows a policy $\pi : \mathcal{S} \times \mathcal{A} \rightarrow [0, 1]$. At each time step $h \in [H]$ in the episode, the agent observes the current state $s_h \in \mathcal{S}$ and selects an action $a_h \sim \pi(\cdot|s_h)$ to execute, then the environment transits to the next state $s_{h+1} \sim \mathbb{P}(\cdot|s_h, a_h)$, yielding an immediate reward $r_h = r(s_h, a_h)$. At step h in the episode, the action-value $Q(s_h, a_h)$ approximates the long-term return $\sum_{t=h}^H \gamma^{t-h} r_t$ after executing action a_h at state s_h and following policy π thereafter, where $0 \leq \gamma < 1$ is the discount parameter.

Currently, many algorithms have been developed to learn the optimal policy π^* for the agent to select and execute actions at each time step h in the episode, thus ultimately maximizing the long-term return $\sum_{h=1}^H \gamma^{h-1} r_h$. Notable algorithms include DQN (Mnih et al., 2015), PPO (Schulman et al., 2017), SAC (Haarnoja et al., 2018), IMPALA (Espeholt et al., 2018), DSAC (Duan et al., 2021; 2023), etc.

Observation 3.1. A common component of existing algorithms is the use of a network to approximate the action-value function¹ Q under a specific policy as Equation 1, where $\phi(\cdot, \cdot|\mathbf{W})$ is the embedding layers, θ and \mathbf{W} are trainable parameters of the network.

$$Q(s, a) = \theta^T \phi(s, a|\mathbf{W}). \quad (1)$$

Bellman equation (Mnih et al., 2015) is employed to update the action-value function. Using the most recent action-value function, the policy can be updated in various ways, depending on the specific algorithm. Since CAE focuses on leveraging Equation 1 for efficient exploration while preserving the core techniques of existing algorithms, we introduce CAE within the context of DQN for simplicity. However, it can be easily adapted to other RL algorithms.

3.2. CAE: the Critic as an Explorer

For a state-action pair (s, a) , the approximated action-value $Q(s, a)$ is subject to an uncertainty term $\beta(s, a)$, arising from the novelty or limited experience with the particular

¹In some algorithms, the state- instead of the action-value functions are learned. However, this does not affect the implementation and conclusion of our method, as will be seen in Section 3.2.

Table 2. Comparison of exploration methods on MiniHack tasks. **Networks**: additional networks required beyond those in IMPALA, which contains 25,466,652 parameters; **Parameters**: the number of additional parameters introduced by the exploration method. Networks in **bold** represent those with significant parameters, while those in *gray* indicate substantially fewer parameters.

Algorithm	Networks	Parameters	Parameter increase
ICM	Embedding net + Forward dynamics net + Inverse dynamics net	16,074,512 + 2,110,464 + 527,371	73%
RND	Embedding net	16,074,512	63%
RIDE	Embedding net + Forward dynamics net + Inverse dynamics net	16,074,512 + 2,110,464 + 527,371	73%
NovelD	Embedding net	16,074,512	63%
E3B	Embedding net + Inverse dynamics net	16,074,512 + 527,371	65%
CAE	-	-	0%
CAE+	Inverse dynamics net	199,819	0.8%

state-action pair. Similar to MAB problems, it is essential to account for this uncertainty when utilizing the latest approximated action-value function. Incorporating the uncertainty term encourages exploration, ultimately improving long-term performance. Consequently, the action-value function adjusted for uncertainty is as Equation 2, where $\alpha \geq 0$ is the exploration coefficient. Notably, in some literature, *uncertainty* is also referred to as a *bonus*, and we use these terms interchangeably when unambiguous.

$$Q(s, a) = \theta^\top \phi(s, a | \mathbf{W}) + \alpha \beta(s, a) \quad (2)$$

However, defining $\beta(s, a)$ remains a significant challenge. Traditional MAB methods often attempt to address this by either assuming a linear action-value function or relying on algorithms (Yang et al., 2020) that require $O(n^3)$ computation time in terms of the number of parameters n in the action-value network. Both of these approaches have inherent drawbacks. Linearity may fail to capture the complexity of real-world tasks. On the other hand, algorithms with $O(n^3)$ computation time become impractical.

To overcome these limitations, we draw inspiration from Neural-LinUCB (Xu et al., 2022) and Neural-LinTS (Riquelme et al., 2018), which effectively decouple representation learning from exploration. Building on this idea and following the standard value network structure in Equation 1, CAE adopts a similar approach by decomposing the action-value function into two distinct components.

- Network $\phi(s, a | \mathbf{W})$ extracts the embedding of the state-action pair (s, a) ;
- $Q(s, a) = \theta^\top \phi(s, a | \mathbf{W})$ is a linear function of the embedding of (s, a) , where θ is the parameter vector.

Consequently, MAB theory with the linearity assumption can be applied to the embeddings $\phi(s, a)$ for $\forall s \in \mathcal{S}$ and $\forall a \in \mathcal{A}$. Simultaneously, the action-value function retains its representational capacity through the embedding layers $\phi(s, a)$, ensuring promising empirical performance. While

any linear MAB technique can be applied to the embeddings, we focus on discussing the two most representative ones as illustrations, noting that others can be utilized similarly.

Upper Confidence Bound (UCB) is an optimistic exploration strategy in MAB. It defines the uncertainty term as Equation 3, where \mathbf{A} is the variance matrix and initialized as $\mathbf{A} = \mathbf{I}$. After each time step executing action a under state s , \mathbf{A} is updated according to Equation 4.

$$\beta(s, a) = \sqrt{\phi(s, a)^\top \mathbf{A}^{-1} \phi(s, a)} \quad (3)$$

$$\mathbf{A} \leftarrow \mathbf{A} + \phi(s, a) \phi^\top(s, a) \quad (4)$$

Thompson Sampling samples the value function adjusted for uncertainty from a posterior distribution. It defines the uncertainty term as Equation 5, where the variance matrix \mathbf{A} is determined and updated in the same manner as in UCB.

$$\begin{aligned} \Delta \theta &\sim N(0, \mathbf{A}^{-1}) \\ \beta(s, a) &= (\Delta \theta)^\top \phi(s, a) \end{aligned} \quad (5)$$

As the value network undergoes continuous updates, exploration based on its embedding layers $\phi(\cdot, \cdot)$ becomes highly unstable, significantly impairing practical performance. Inspired by existing scaling strategies (Welford, 1962; Elsayed et al., 2024), we adopt an appropriate one for the generated uncertainty at each time step, ensuring both stability and practical functionality, as detailed in Algorithm 1. This scaling strategy normalizes the generated uncertainty at each time step using the running variance, which, despite its simplicity, has a profound impact on the performance of CAE. The critical importance of this design is further highlighted through ablation studies presented in Section 5.

Adapting CAE to General RL Algorithms. Depending on the RL algorithm employed, we may sometimes learn the state- instead of the action-value network. As a result, the value network can only derive state embeddings rather than state-action pair embeddings. Even when learning the

Algorithm 1 Scaling strategy for the bonus

- 1: **Input:** Bonus b , running mean μ , running variance ν^2 , and running count of samples \mathcal{N}
- 2: Update the sample count $\mathcal{N} \leftarrow \mathcal{N} + 1$
- 3: Compute $\delta = b - \mu$
- 4: Update the running mean $\mu \leftarrow \mu + \frac{\delta}{\mathcal{N}}$
- 5: Update the running variance $\nu^2 \leftarrow \nu^2 + \frac{\delta \times (b - \mu)}{\mathcal{N}}$
- 6: **Output:** Scaled bonus $\frac{b}{\nu}$, and updated μ , ν^2 , and \mathcal{N}

action-value network, it may still output only state embeddings if it is designed to take states as input and produce action values for each action. In such cases, the embedding of the next state can be utilized to replace the embedding of the current state-action pair when generating uncertainty.

3.3. CAE+: Enhancing CAE with Minimal Overhead

For tasks with complex dynamics or sparse rewards, learning well-performing value networks is particularly challenging, which further impedes exploration reliant on them. Accordingly, we propose CAE+, an extension incorporating a small auxiliary network, adding less than 1% to the parameter count. Specifically, we utilize the Inverse Dynamics Network (IDN) (Pathak et al., 2017; Raileanu & Rocktäschel, 2020; Henaff et al., 2022) to enhance the learning of the embedding layers contained in the action-value network. This is achieved by a compact network f that infers the distribution $p(a_h)$ over actions given consecutive states s_h and s_{h+1} , which is trained by maximum likelihood estimation as Equation 6.

$$L_f = -\log p(a_h | s_h, s_{h+1}) \quad (6)$$

To introduce this enhancement with minimal additional parameters, we utilize the embedding layers. For an action-value network with embedding layers $\phi(s, a)$, a constant default value is assigned to the action input, while the actual states are used as inputs. The resulting outputs are treated as state embeddings. For a state-value network with embedding layers $\phi(s)$, states are input to generate state embeddings. These state embeddings are then transformed by a linear layer parameterized by \mathbf{U} , followed by a small network \bar{f} , which processes the transformed consecutive embeddings to infer the action. Equation 7 provides an example where the embedding layers are $\phi(s, a)$, and \bar{a} represents the default value assigned to the action input.

$$\begin{aligned} p(a_h | s_h, s_{h+1}) &= f(\phi(s_h, \bar{a}), \phi(s_{h+1}, \bar{a})) \\ &= \bar{f}(\mathbf{U}\phi(s_h, \bar{a}), \mathbf{U}\phi(s_{h+1}, \bar{a})) \end{aligned} \quad (7)$$

Accordingly, Equation 3, Equation 4, and Equation 5, which generate the uncertainty in CAE, are updated in CAE+

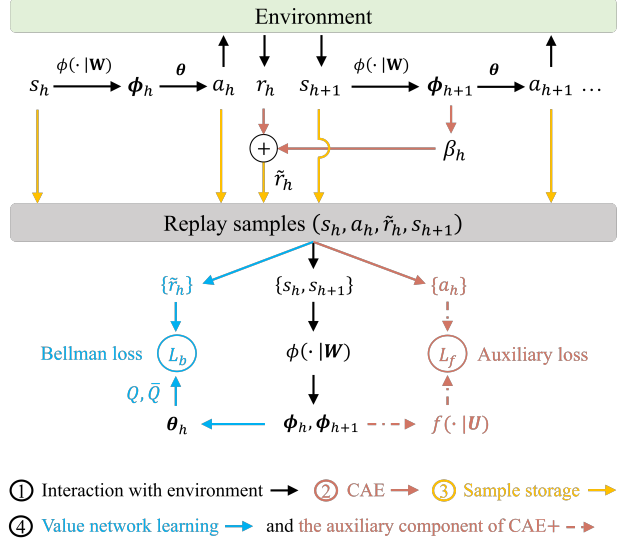


Figure 2. CAE+ with state-value function. L_b represents the Bellman loss used to update the action-value function, while L_f refers to the loss of the auxiliary network, which is detailed in Equation 6.

to Equation 8, Equation 9, and Equation 10, respectively. Algorithm 2 provides a detailed summary of CAE+ with action-value network, while Figure 2 illustrates its overall framework when applied with state-value network.

$$\beta(s, a) = \sqrt{\phi(s, a)^\top \mathbf{U}^\top \mathbf{A}^{-1} \mathbf{U} \phi(s, a)} \quad (8)$$

$$\mathbf{A} \leftarrow \mathbf{A} + \mathbf{U} \phi(s, a) \phi^\top(s, a) \mathbf{U} \quad (9)$$

$$\beta(s, a) = (\Delta \theta)^\top \mathbf{U} \phi(s, a) \quad (10)$$

In CAE+, the structure of network f brings several advantages. First, the incorporation of \mathbf{U} effectively decouples the action-value network from the environment dynamics, reducing interdependencies that could hinder learning and thereby improving empirical performance, as demonstrated through ablation studies in Section 5. Second, since \mathbf{U} is a simple linear transformation, it also retains the theoretical guarantees of UCB- and Thompson Sampling-based exploration strategies, maintaining the rigor and stability of the exploration process. Third, by transforming $\phi(s, a)$ into a lower-dimensional embedding with $\bar{d} < d$, the design not only minimizes the number of additional parameters but also reduces the computational complexity of uncertainty calculation at each time step from $O(d^3)$ to $O(\bar{d}^3)$, making the method efficient and scalable for practical applications.

Speed Up CAE+ with Rank-1 Update. According to Algorithm 2, the variance matrix \mathbf{A} needs to be inverted at each step, an operation that is cubic in dimension \bar{d} . **Alternatively**, we can use the Sherman-Morrison matrix identity

Algorithm 2 CAE+ with action-value network

- 1: **Input:** Ridge parameter $\lambda > 0$, exploration parameter $\alpha \geq 0$, episode length H , episode number M
- 2: **Initialize:** Covariance matrix $\mathbf{A} = \lambda \mathbf{I}$, initial policy $\pi(\cdot)$ and action-value function $Q(\cdot, \cdot)$, impact network $f(\cdot | \mathbf{U})$
- 3: **for** episode $m = 1$ **to** M **do**
- 4: Receive the initial state s_1^m from the environment
- 5: **for** step $h = 1, 2, \dots, H$ **do**
- 6: Conduct action $a_h^m \sim \pi(s_h^m)$ and observe the next state s_{h+1}^m and receive immediate reward r_h^m
- 7: Generate bonus $\beta(s_h^m, a_h^m)$ by Equation 8 or 10, etc.
- 8: Scale the bonus $\beta(s_h^m, a_h^m)$ to get β_h^m by Algorithm 1
- 9: Reshape the reward $\tilde{r}_h^m = r_h^m + \alpha \beta_h^m$
- 10: Update the covariance matrix \mathbf{A} by Equation 9
- 11: **end for**
- 12: Sample a batch $\mathcal{B} = \{s_h, a_h, s_{h+1}, \tilde{r}_h\}, h \in [1, H - 1]$
- 13: Calculate the IDN loss L_f by Equation 6 and 7 on \mathcal{B}
- 14: Update the value function $Q(\cdot, \cdot)$ and network f by Equation 12, where L_b is the Bellman loss of $Q(\cdot, \cdot)$ on \mathcal{B}

$$\min(L_b + L_f) \quad (12)$$
- 15: Update the policy $\pi(\cdot)$
- 16: **end for**

(Sherman & Morrison, 1950; Henaff et al., 2022) to perform rank-1 updates of \mathbf{A}^{-1} in quadratic time as Equation 11.

$$\mathbf{A}^{-1} \leftarrow \mathbf{A}^{-1} - \frac{\mathbf{A}^{-1} \mathbf{U} \phi(s, a) \phi^\top(s, a) \mathbf{U}^\top (\mathbf{A}^{-1})^\top}{1 + \phi^\top(s, a) \mathbf{U}^\top \mathbf{A}^{-1} \mathbf{U} \phi(s, a)} \quad (11)$$

4. Theoretical Analysis

Under the true optimal policy π^* , assume the corresponding action-value function Q^* is structured as in Equation 1 and parameterized by θ^* and \mathbf{W}^* . In Algorithm 2, the policy executed in episode $m \in [M]$ is denoted by π_m , with its action-value function represented as Q^{π_m} . Cumulative regret of Algorithm 2 is as Definition 4.1.

Definition 4.1. Cumulative Regret. After M episodes of interactions with the environment, the cumulative regret of Algorithm 2 is defined as Equation 13, where u_1^m is the optimal action at state s_1^m generated by policy π^* while a_1^m is that selected by the executed policy π_m .

$$\text{Reg}_M = \sum_{m=1}^M Q^*(s_1^m, u_1^m) - Q^{\pi_m}(s_1^m, a_1^m) \quad (13)$$

Cumulative regret quantifies the gap between the optimal return and the actual return accumulated over M episodes of interaction with the environment. CAE draws inspiration from Neural-LinUCB (Xu et al., 2022) and Neural-LinTS (Riquelme et al., 2018). However, while Neural-LinUCB

is supported by theoretical analysis, Neural-LinTS has only been validated empirically. In this work, we complete the regret bound for Neural-LinTS in Appendix D.2, leading us to the regret bound for Algorithm 2, as stated in Theorem 4.2.

Theorem 4.2. *Suppose the standard assumptions from the literature (Yang et al., 2020; Xu et al., 2022) hold, $\|\theta^*\|_2 \leq 1$ and $\|(s_h; a_h)\|_2 \leq 1$. For any $\sigma \in (0, 1)$, assume the number of parameters in each of the L layers of $\phi(\cdot, \cdot)$ satisfies $\iota = \text{poly}(L, d, \frac{1}{\sigma}, \log \frac{M|\mathcal{A}|}{\sigma})$, where $|\mathcal{A}|$ means the action space size and $\text{poly}(\cdot)$ means a polynomial function depending on the incorporated variables. Let:*

$$\begin{aligned} \alpha &= \sqrt{2(d \cdot \log(1 + \frac{M \cdot \log |\mathcal{A}|}{\lambda}) - \log \sigma) + \sqrt{\lambda}} \\ \eta &\leq C_1(\iota \cdot d^2 M^{\frac{11}{2}} L^6 \cdot \log \frac{M|\mathcal{A}|}{\sigma})^{-1} \end{aligned} \quad (14)$$

then with probability at least $1 - \sigma$, it holds that:

$$\begin{aligned} \text{Reg}_M &\leq C_2 \alpha H \sqrt{Md \log(1 + \frac{M}{\lambda d})} + C_4 H \sqrt{MH \log \frac{2}{\sigma}} \\ &\quad + \frac{C_3 H L^3 d^{\frac{5}{2}} M \sqrt{\log(\iota + \frac{1}{\sigma} + \frac{M|\mathcal{A}|}{\sigma})} \|\mathbf{q} - \tilde{\mathbf{q}}\|_{\mathbf{H}^{-1}}}{\iota^{\frac{1}{6}}} \end{aligned}$$

where C_1, C_2, C_3, C_4 are constants; \mathbf{q} and $\tilde{\mathbf{q}}$ are the target value vector and the estimated value vector of the action-value network, respectively; \mathbf{H} is the neural tangent kernel, as defined in Neural-LinUCB (Xu et al., 2022).

Specifically, we assume $\|\theta^*\|_2 \leq 1$ and $\|(s_h; a_h)\|_2 \leq 1$ to make the bound scale-free. Neural tangent kernel \mathbf{H} is defined in accordance with a recent line of research (Jacot et al., 2018; Arora et al., 2019) and is essential for the analysis of overparameterized neural networks. Other standard assumptions and initialization are explained in Appendix D.1. From this theorem, we can conclude that the upper bound of the cumulative regret grows sub-linearly with the number of episodes M , i.e., $\tilde{O}(\sqrt{M})$ where $\tilde{O}(\cdot)$ hide constant and logarithmic dependence of M , indicating that the executed policy improves over time. Notably, the last term in the bound arises from the error due to network estimation. Here, M can be traded off against ι and the estimation error $\|\mathbf{q} - \tilde{\mathbf{q}}\|_{\mathbf{H}^{-1}}$, making it often neglected.

5. Experiment

In this section, we evaluate CAE and CAE+ on tasks from MuJoCo and MiniHack, which feature dense and sparse rewards, respectively. For the MuJoCo tasks, which are characterized by dense rewards, we examine four state-of-the-art deep RL algorithms: SAC (Haarnoja et al., 2018), PPO (Schulman et al., 2017), TD3 (Fujimoto et al., 2018),

Table 3. Experimental results after 1e6 interaction steps on MuJoCo-v4 tasks, except for the *Humanoid* task, whose results are evaluated after 4e6 interaction steps. *RPI* represents the **Relative Performance Improvement** achieved by CAE.

Env \ Algorithm	PPO	PPO + CAE	<i>RPI</i>	TD3	TD3 + CAE	<i>RPI</i>	SAC	SAC + CAE	<i>RPI</i>
Swimmer	99 ± 11.5	107 ± 6.47	8.08%	78 ± 15.4	130 ± 14.2	66.7%	61 ± 35.2	161 ± 26.9	164%
Hopper	2503 ± 786.6	2453 ± 673.2	-2.00%	3044 ± 574.0	3244 ± 226.3	6.57%	2908 ± 600.8	3188 ± 485.2	9.63%
Walker2d	3405 ± 842.0	3554 ± 928.0	4.38%	3764 ± 234.4	4251 ± 567.1	12.9%	4362 ± 405.5	4742 ± 484.4	8.71%
Ant	1762 ± 540.0	2378 ± 843.4	35.0%	3492 ± 1745.7	5074 ± 519.3	45.3%	4846 ± 1306.4	5482 ± 511.9	13.1%
HalfCheetah	2636 ± 1344.3	3104 ± 926.0	17.8%	10316 ± 193.8	10473 ± 563.4	1.52%	11154 ± 457.1	11587 ± 418.3	3.88%
Humanoid	619 ± 92.1	646 ± 127.1	4.36%	5973 ± 257.7	6275 ± 483.2	5.06%	5261 ± 186.4	5218 ± 228.4	-0.82%
<i>RPI Mean</i>	-	-	11.3%	-	-	23.0%	-	-	33.1%

and DSAC (Duan et al., 2021; 2023), both with and without CAE. For the MiniHack tasks, we use IMPALA (Espeholt et al., 2018) as the base RL algorithm due to its effectiveness and frequent use in sparse reward tasks. We compare CAE+ against E3B (Henaff et al., 2022), which has been shown to outperform several exploration baselines such as ICM (Pathak et al., 2017), RND (Burda et al., 2019b), RIDE (Raileanu & Rocktäschel, 2020), NovelD (Zhang et al., 2021a), and others. The results for these baselines are documented in the E3B paper and are reproducible using its released codebase. Notably, these baselines **rarely achieve positive performance** on MiniHack tasks without human engineering. For this reason, we do not replicate their experiments or restate their results in this paper.

Reproducibility. All the experiments are based on publicly available codebases from E3B (Henaff et al., 2022), CleanRL (Huang et al., 2022), and DSAC (Duan et al., 2021; 2023). Core code and detailed hyperparameters are provided in Appendix A and Appendix E, respectively.

5.1. MuJoCo tasks with Dense Rewards

MuJoCo testbed is a widely used physics-based simulation environment for benchmarking RL algorithms. MuJoCo provides a suite of continuous control tasks where agents must learn to perform various actions, such as locomotion, manipulation, and balancing, within simulated robotic environments. Since comparisons among state-of-the-art RL baselines, such as PPO, SAC, TD3, and DSAC on MuJoCo, have been extensively covered in previous studies, our focus is on investigating how CAE can enhance these algorithms. Thus, we concentrate on comparing the performance of each specific algorithm with and without CAE.

Experimental results are summarized in Table 3, using seeds {1, 2, 3, 4, 5}. The results demonstrate that CAE consistently improves the performance of PPO, TD3, and SAC across most MuJoCo tasks. Notably, TD3 and SAC, when enhanced with CAE, show significantly better performance on the *Swimmer* task. While this task is not typically regarded as particularly challenging, standalone implementations of TD3 and SAC have achieved limited performance.

Table 4. Experimental results after 1e6 steps on MuJoCo-v3, except for *Humanoid*, whose results are evaluated after 2e6 steps.

Env \ Algorithm	DSAC	DSAC + CAE	<i>RPI</i>
Swimmer	131 ± 14.8	150 ± 7.96	14.5%
Hopper	2417 ± 541.6	2845 ± 594.5	17.7%
Walker2d	5550 ± 624.0	6069 ± 422.1	9.35%
Ant	5912 ± 809.7	6305 ± 322.7	6.65%
HalfCheetah	16036 ± 439.1	16338 ± 249.1	1.88%
Humanoid	10059 ± 996.1	10333 ± 1104.4	2.72%
<i>RPI Mean</i>	-	-	8.80%

In Table 4, we summarize the results of DSAC with and without CAE. It is worth noting that the experiments with DSAC are conducted on MuJoCo-v3 instead of MuJoCo-v4 solely because the publicly available DSAC codebase is based on MuJoCo-v3, with no other underlying reasons. As shown, CAE also enhances the performance of DSAC on the MuJoCo benchmark. For detailed figures of the experimental results in this subsection, refer to Appendix E.

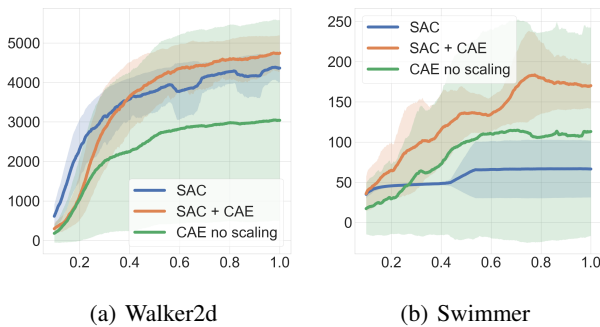


Figure 3. Ablation study to the *scaling strategy* on MuJoCo. The horizontal axis denotes the number of steps, in multiples of 1e6.

Ablation study to the *scaling strategy* in Algorithm 1. Additionally, we conduct experiments to assess the necessity of the scaling strategy. Experiment results, illustrated in Figure 3, are based on randomly selected tasks for SAC. As shown, SAC enhanced with CAE fails to deliver satisfactory

Table 5. Experimental results after $2e7 - 3e7$ interaction steps on MiniHack tasks, including *MultiRoom-N4*, *MultiRoom-N4-Locked*, *MultiRoom-N6*, *MultiRoom-N6-Locked*, *MultiRoom-N10-OpenDoor*, *Freeze-Horn-Restricted*, *Freeze-Random-Restricted*, *Freeze-Wand-Restricted*, and *LavaCross-Restricted*, with varying levels of difficulty. *RPI* quantifies the improvement of CAE+ compared to E3B.

Algorithm \ Env	N4	N4-Locked	N6	N6-Locked	N10-OpenDoor	Horn	Random	Wand	LavaCross
E3B	0.86 ± 0.010	0.72 ± 0.090	0.77 ± 0.041	-0.31 ± 0.403	0.71 ± 0.042	0.47 ± 0.071	0.57 ± 0.071	0.49 ± 0.201	0.22 ± 0.412
CAE	0.93 ± 0.014	0.84 ± 0.041	-0.45 ± 0.222	-0.37 ± 0.310	-0.84 ± 0.216	0.92 ± 0.022	0.93 ± 0.022	0.93 ± 0.030	0.16 ± 0.394
CAE+	0.97 ± 0.006	0.87 ± 0.017	0.94 ± 0.016	0.77 ± 0.093	0.86 ± 0.023	0.84 ± 0.055	0.80 ± 0.040	0.65 ± 0.131	0.84 ± 0.024
<i>RPI</i>	12.79%	20.83%	22.08%	348.39%	21.13%	78.72%	40.35%	32.65%	281.82%

performance on *Walker2d* and *Swimmer* tasks when the scaling strategy is not applied. It achieves high performance under certain seeds, while it performs poorly under others, leading to poor overall results and large variance. This highlights the critical role of the scaling strategy in ensuring the practical stability and effectiveness of CAE.

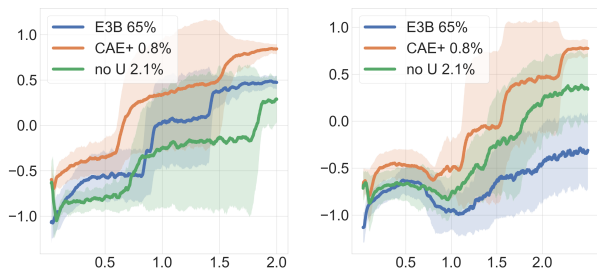
5.2. MiniHack tasks with Sparse Rewards

MiniHack (Samvelyan et al., 2021) is built on the NetHack Learning Environment (Küttler et al., 2020), a challenging video game where an agent navigates procedurally generated dungeons to retrieve a magical amulet. MiniHack tasks present a diverse set of challenges, such as locating and utilizing magical objects, traversing hazardous environments like lava, and battling monsters. These tasks are characterized by sparse rewards, and the state provides a wealth of information, including images, text, and more, though only a subset is relevant to each specific task.

As shown in Table 2, CAE+ introduces only a 0.8% increase in parameters compared to IMPALA, which lacks a dedicated exploration module. In contrast, other exploration baselines, such as RIDE and E3B, require 60% – 80% additional parameters over IMPALA, highlighting the lightweight design of CAE+. Experimental results for E3B and CAE+, using seeds $\{1, 2, 3\}$, are summarized in Table 5, where their performance is evaluated across representative tasks: five *navigation* tasks and four *skill* tasks. The results demonstrate that CAE+ consistently outperforms E3B. Notably, for challenging tasks such as *MultiRoom-N6-Locked* and *LavaCross-Restricted*, CAE+ achieves remarkable improvements of 348% and 282%, respectively. For detailed experimental figures, refer to Appendix E.

Ablation study to CAE on MiniHack. Results of CAE on MiniHack tasks are provided in Table 5. As shown, CAE successfully solves a subset of tasks and even surpasses CAE+ in certain cases. However, it struggles to achieve positive performance in others, such as *MultiRoom-N6-Locked* and *MultiRoom-N10-OpenDoor*, etc., which pose significant exploration challenges. This limitation stems from the difficulty of training effective value networks in complex environments, adversely affecting exploration reliant on them. These observations highlight the importance of CAE+.

Ablation study to the transformation U . Additionally, we present experimental results for CAE+ without the transformation matrix U in the auxiliary network f . As shown in Figure 4, CAE+ without U occasionally outperforms E3B, though there are instances where it does not. Importantly, it consistently underperforms compared to the full CAE+ with U . Moreover, CAE+ introduces more additional parameters without U , specifically 2.1%.



(a) Freeze-Horn-Restricted (b) MultiRoom-N6-Locked

Figure 4. Ablation study to U on MiniHack tasks. The horizontal axis denotes the number of interaction steps, in multiples of $1e7$.

6. Conclusion

In this paper, we propose CAE, a lightweight exploration method that integrates seamlessly with existing RL algorithms without introducing additional parameters. CAE leverages the embedding layers of the value network within the RL algorithm to drive exploration, leaving the rest of the algorithm unchanged. Its stability and practicality are ensured through an effective scaling strategy. For tasks with sparse rewards, we extend CAE to CAE+ by incorporating a small auxiliary network, which accelerates learning with a minimal increase in parameters. We provide theoretical guarantees for CAE and CAE+, establishing a sub-linear regret bound based on the number of interaction episodes and demonstrating their sample efficiency. Experimental evaluations on the MuJoCo and MiniHack benchmarks, across dense and sparse reward settings, show that CAE and CAE+ consistently outperform state-of-the-art baselines, effectively bridging the gap between theoretical soundness and practical efficiency in RL exploration.

Impact Statement

In this paper, we bridge the gap between provably efficient and empirically successful exploration methods. While provably efficient approaches often struggle with practical limitations, empirically driven methods typically lack theoretical guarantees and demand extensive parameter training. Inspired by the *deep representation and shallow exploration* paradigm, we introduce a novel framework that decomposes value networks in deep RL and repurposes them for exploration, achieving theoretical guarantees with minimal or no additional parameter training. This approach seamlessly integrates any linear MAB technique into deep RL algorithms by leveraging the embeddings of value networks. Future work could investigate the application of additional linear MAB techniques beyond the two adopted in this study and evaluate the proposed framework across a wider range of benchmarks to further validate and enhance its effectiveness.

References

- Agarwal, A., Kakade, S., Henaff, M., and Sun, W. Pcp: Policy cover directed exploration for provable policy gradient learning. In *Advances in Neural Information Processing Systems*, 2020.
- Agrawal, S. and Goyal, N. Thompson sampling for contextual bandits with linear payoffs. In *Proceedings of the 30th International Conference on Machine Learning*, pp. 127–135. PMLR, 2013.
- Arora, S., Du, S. S., Hu, W., Li, Z., Salakhutdinov, R., and Wang, R. On exact computation with an infinitely wide neural net. In *Advances in Neural Information Processing Systems*, 2019.
- Ash, J. T., Zhang, C., Goel, S., Krishnamurthy, A., and Kakade, S. Anti-concentrated confidence bonuses for scalable exploration. In *Proceedings of the 10th International Conference on Learning Representations*, 2022.
- Bellemare, M. G., Srinivasan, S., Ostrovski, G., Schaul, T., Saxton, D., and Munos, R. Unifying count-based exploration and intrinsic motivation. In *Advances in Neural Information Processing Systems*, 2016.
- Burda, Y., Edwards, H., Pathak, D., Storkey, A., Darrell, T., and Efros, A. A. Large-scale study of curiosity-driven learning. In *Proceedings of the 7th International Conference on Learning Representations*, 2019a.
- Burda, Y., Edwards, H., Storkey, A., and Klimov, O. Exploration by random network distillation. In *Proceedings of the 7th International Conference on Learning Representations*, 2019b.
- Cai, Q., Yang, Z., Jin, C., and Wang, Z. Provably efficient exploration in policy optimization. In *Proceedings of the 37th International Conference on Machine Learning*, 2020.
- Chowdhury, S. R. and Gopalan, A. On kernelized multi-armed bandits. In *Proceedings of the 34th International Conference on Machine Learning*. PMLR, 2017.
- Chu, W., Li, L., Reyzin, L., and Schapire, R. E. Contextual bandits with linear payoff functions. In *Proceedings of the 14th International Conference on Artificial Intelligence and Statistics*, pp. 208–214, 2011.
- Duan, J., Guan, Y., Li, S., Ren, Y., Sun, Q., and Cheng, B. Distributional soft actor-critic: Off-policy reinforcement learning for addressing value estimation errors. *IEEE Transactions on Neural Networks and Learning Systems*, pp. 6584 – 6598, 2021.
- Duan, J., Wang, W., Xiao, L., Gao, J., and Li, S. Dsac-t: Distributional soft actor-critic with three refinements. *arXiv:2310.05858v4*, 2023.
- Elsayed, M., Vasan, G., and Mahmood, A. R. Deep reinforcement learning without experience replay, target networks, or batch updates. *38th Workshop on Fine-Tuning in Machine Learning, NeurIPS*, 2024.
- Espeholt, L., Soyer, H., Munos, R., Simonyan, K., Mnih, V., Ward, T., Doron, Y., Firoiu, V., Harley, T., Dunning, I., Legg, S., and Kavukcuoglu, K. Impala: Scalable distributed deep-rl with importance weighted actor-learner architectures. In *Proceedings of the 35th International Conference on Machine Learning*. PMLR, 2018.
- Flet-Berliac, Y., Ferret, J., Pietquin, O., Preux, P., and Geist, M. Adversarially guided actor-critic. In *Proceedings of the 9th International Conference on Learning Representations*, 2021.
- Fujimoto, S., Hoof, H. v., and Meger, D. Addressing function approximation error in actor-critic methods. In *Proceedings of the 35th International Conference on Machine Learning*. PMLR, 2018.
- Haarnoja, T., Zhou, A., Abbeel, P., and Levine, S. Soft actor-critic: Off-policy maximum entropy deep reinforcement learning with a stochastic actor. In *Proceedings of the 35th International Conference on Machine Learning*. PMLR, 2018.
- Henaff, M., Raileanu, R., Jiang, M., and Rocktäschel, T. Exploration via elliptical episodic bonuses. In *Advances in Neural Information Processing Systems*, 2022.
- Henaff, M., Jiang, M., and Raileanu, R. A study of global and episodic bonuses for exploration in contextual mdp.

- In *Proceedings of the 40th International Conference on Machine Learning*. PMLR, 2023.
- Huang, S., Dossa, R. F. J., Ye, C., Braga, J., Chakraborty, D., Mehta, K., and Araújo, J. G. Cleanrl: High-quality single-file implementations of deep reinforcement learning algorithms. *Journal of Machine Learning Research*, pp. 1–18, 2022.
- Ishfaq, H., Cui, Q., Nguyen, V., Ayoub, A., Zhuoran, Y., Wang, Z., Precup, D., and Yang, F. L. Randomized exploration for reinforcement learning with general value function approximation. In *Proceedings of the 38th International Conference on Machine Learning*, 2021.
- Ishfaq, H., Lan, Q., Xu, P., Mahmood, A. R., Precup, D., Anandkumar, A., and Azizzadenesheli, K. Provable and practical: Efficient exploration in reinforcement learning via langevin monte carlo. In *Proceedings of the 12nd International Conference on Learning Representations*, 2024a.
- Ishfaq, H., Tan, Y., Yang, Y., Lan, Q., Lu, J., Mahmood, A. R., Precup, D., and Xu, P. More efficient randomized exploration for reinforcement learning via approximate sampling. In *Proceedings of the 1st Reinforcement Learning Conference*, 2024b.
- Jacot, A., Gabriel, F., and Hongler, C. Neural tangent kernel: Convergence and generalization in neural networks. In *Advances in Neural Information Processing Systems*, 2018.
- Jarrett, D., Tallec, C., Alché, F., Mesnard, T., Munos, R., and Valko, M. Curiosity in hindsight: Intrinsic exploration in stochastic environments. In *Proceedings of the 40th International Conference on Machine Learning*. PMLR, 2023.
- Jin, C., Allen-Zhu, Z., Bubeck, S., and Jordan, M. I. Is q-learning provably efficient? In *Advances in Neural Information Processing Systems*, 2018.
- Jin, C., Yang, Z., Wang, Z., and Jordan, M. I. Provably efficient reinforcement learning with linear function approximation. In *In Conference on Learning Theory*. PMLR, 2020.
- Kearns, M. and Singh, S. Near-optimal reinforcement learning in polynomial time. *Machine Learning*, 2002.
- Küttler, H., Nardelli, N., Miller, A. H., Raileanu, R., Selvatici, M., Grefenstette, E., and Rocktäschel, T. The nethack learning environment. In *Advances in Neural Information Processing Systems*, 2020.
- Li, L., Chu, W., Langford, J., and Schapire, R. E. A contextual-bandit approach to personalized news article recommendation. In *Proceedings of the 19th International Conference on World Wide Web*, pp. 661–670, 2010.
- Li, Y., Mu, Z., and Qi, S. A contextual combinatorial bandit approach to negotiation. In *Proceedings of the 41st International Conference on Machine Learning*, 2024.
- Lillicrap, T. P., Hunt, J. J., Pritzel, A., Heess, N., Erez, T., Tassa, Y., Silver, D., and Wierstra, D. Continuous control with deep reinforcement learning. In *Proceedings of the 4th International Conference on Learning Representations*, 2016.
- Mnih, V., Kavukcuoglu, K., Silver, D., Graves, A., Antonoglou, I., Wierstra, D., and Riedmiller, M. Playing atari with deep reinforcement learning. *arXiv preprint arXiv: 1312.5602v1*, 2013.
- Mnih, V., Kavukcuoglu, K., Silver, D., Rusu, A. A., Veness, J., Bellemare, M. G., Graves, A., Riedmiller, M., Fidjeland, A. K., Ostrovski, G., Petersen, S., Beattie, C., Sadik, A., Antonoglou, I., King, H., Kumaran, D., Wierstra, D., Legg, S., and Hassabis, D. Human-level control through deep reinforcement learning. *nature*, pp. 529–533, 2015.
- Osband, I., Roy, V. B., and Wen, Z. Generalization and exploration via randomized value functions. In *Proceedings of the 33rd International Conference on Machine Learning*. PMLR, 2016.
- Osband, I., Roy, V. B., Russo, J. D., and Wen, Z. Deep exploration via randomized value functions. *Journal of Machine Learning Research*, pp. 1–61, 2019.
- Pathak, D., Agrawal, P., Efros, A. A., and Darrell, T. Curiosity-driven exploration by self-supervised prediction. In *Proceedings of the 34th International Conference on Machine Learning*. PMLR, 2017.
- Raileanu, R. and Rocktäschel, T. Ride: Rewarding impact-driven exploration for procedurally-generated environments. In *Proceedings of the 8th International Conference on Learning Representations*, 2020.
- Riquelme, C., Tucker, G., and Snoek, J. Deep bayesian bandits showdown: An empirical comparison of bayesian deep networks for thompson sampling. In *Proceedings of the 6th International Conference on Learning Representations*, 2018.
- Samvelyan, M., Kirk, R., Kurin, V., Parker-Holder, J., Jiang, M., Hambro, E., Petroni, F., Kuttler, H., Grefenstette, E., and Rocktäschel, T. Minihack the planet: A sandbox for open-ended reinforcement learning research. In *Advances in Neural Information Processing Systems*, 2021.

- Schulman, J., Wolski, F., Dhariwal, P., Radford, A., and Klimov, O. Proximal policy optimization algorithms. *arXiv preprint arXiv: 1707.06347v2*, 2017.
- Sherman, J. and Morrison, J. W. Adjustment of an inverse matrix corresponding to a change in one element of a given matrix. *The Annals of Mathematical Statistics*, 1950.
- Silver, D., Schrittwieser, J., Simonyan, K., Antonoglou, I., Huang, A., Guez, A., Hubert, T., Baker, L., Lai, M., Bolton, A., Chen, Y., and Lillicrap, T. e. a. Mastering the game of go without human knowledge. *Nature*, 2017.
- Valko, M., Korda, N., Munos, R., Flaounas, I., and Cristianini, N. Finite-time analysis of kernelised contextual bandits. *arXiv preprint arXiv: 1309.6869*, 2013.
- Vinyals, O., Babuschkin, I., Czarnecki, W. M., Mathieu, M., Dudzik, A., Chung, J., Choi, D. H., Powell, R., Ewalds, T., and Georgiev, P. e. a. Grandmaster level in starcraft ii using multi-agent reinforcement learning. *Nature*, 2019.
- Welford, B. P. Note on a method for calculating corrected sums of squares and products. *Technometrics*, 1962.
- Wen, Z., Kveton, B., and Ashkan, A. Efficient learning in large-scale combinatorial semi-bandits. In *Proceedings of the 32nd International Conference on Machine Learning*, pp. 1113–1122. PMLR, 2015.
- Xu, P., Wen, Z., Zhao, H., and Gu, Q. Neural contextual bandits with deep representation and shallow exploration. In *Proceedings of the 10th International Conference on Learning Representations*, 2022.
- Yang, Z., Jin, C., Wang, Z., Wang, M., and Jordan, M. I. On function approximation in reinforcement learning: Optimism in the face of large state spaces. In *Advances in Neural Information Processing Systems*, 2020.
- Yuan, M., Li, B., Jin, X., and Zeng, W. Automatic intrinsic reward shaping for exploration in deep reinforcement learning. In *Proceedings of the 40th International Conference on Machine Learning*, pp. 40531–40554. PMLR, 2023.
- Zahavy, T. and Mannor, S. Neural linear bandits: Overcoming catastrophic forgetting through likelihood matching. *arXiv preprint arXiv: 1901.08612v2*, 2019.
- Zhang, T., Xu, H., Wang, X., Wu, Y., Keutzer, K., Gonzalez, J. E., and Tian, Y. Noveld: A simple yet effective exploration criterion. In *Advances in Neural Information Processing Systems*, 2021a.
- Zhang, W., Zhou, D., Li, L., and Gu, Q. Neural thompson sampling. In *Proceedings of the 9th International Conference on Learning Representations*, 2021b.
- Zhou, D., Li, L., and Gu, Q. Neural contextual bandits with ucb-based exploration. In *Proceedings of the 37th International Conference on Machine Learning*, pp. 11492–11502. PMLR, 2020.

A. Implementation

In Listing 1, we present the core code of CAE, while the rest of the deep RL algorithm remains unchanged. As shown, CAE is simple to implement, integrates seamlessly with any existing RL algorithm, and requires no additional parameter learning beyond what is already in the RL algorithm.

Listing 1. CAE core code

```
cov_inverse = torch.inverse(cov) # inverse of covariance matrix
emb = q_net.get_emb(torch.Tensor(obs), torch.Tensor(action)).squeeze().detach() # embedding of the state-action pair
bouns = np.sqrt(torch.matmul(emb.T, torch.matmul(cov_inverse, emb)).item()) # action-value uncertainty
reward += scaled_bonus # reshape the reward
cov += torch.outer(emb, emb) # update the covariance matrix
```

In Listing 2, we present the additional code of CAE+ alongside that of CAE. As shown, CAE+ minimizes an additional loss, specifically the Inverse Dynamics Loss, in addition to the losses from the original RL algorithm.

Listing 2. Additional core code of CAE+

```
emb = q_net.get_emb(torch.Tensor(batch['obs']), torch.Tensor(batch['action'])) # embeddings of state-action pairs in a training batch
current_emb = emb[: -1] # embeddings of the current step
next_emb = emb[1: ] # embeddings of the next step
predict_action = inverse_dynamic_net(current_emb, next_emb) # inferred actions
inverse_dynamics_loss = compute_inverse_dynamics_loss(predict_action, batch['action'][: -1]) # loss

def compute_inverse_dynamics_loss(action, true_action):
    loss=F.nll_loss(F.log_softmax(torch.flatten(action, 0, 1), dim=-1), target=torch.flatten(true_action, 0, 1), reduction='none')
    return torch.sum(torch.mean(loss.view_as(true_action), dim=1))
```

B. Long version of CAE

For a more thorough theoretical analysis, we present the long and theoretical version of CAE in Algorithm 3, where, for conciseness, we denote the embedding of the state-action pair at time step h in episode m as $\phi_h^m = \phi(s_h^m, a_h^m)$. As per the standard notation in the literature on provable algorithms (Jin et al., 2020; Yang et al., 2020), function parameters are not shared across different time steps $h \in [H]$, which is also the case in Algorithm 3. As we can see, the algorithm iteratively updates parameters θ_h and \mathbf{W}_h , learning the two decomposed components of the action-value function in Equation 1 by Bellman equation. Specifically, the parameter θ_h is updated in Line 9 using its closed-form solution (Li et al., 2010), while the extraction network $\phi_h(\cdot, \cdot)$ remains fixed. Afterwards, the extraction network $\phi_h(s, a | \mathbf{W}_h)$ is updated in Line 10, with the parameter θ_h held constant. In this line, η is the learning rate, L_h^m is the Bellman loss function, and s_h^t, a_h^t, r_h^t for $\forall t \in [m]$ and $\forall h \in [H]$ represent historical experiences.

Algorithm 3 DQN enhanced with CAE

- 1: **Input:** Ridge parameter $\lambda > 0$, the exploration parameter $\alpha \geq 0$, episode length H , episode number M
- 2: **Initialize:** Covariance matrix $\mathbf{A}_h^1 = \lambda \mathbf{I}$, $\mathbf{b}_h^1 = \mathbf{0}$, parameters $\theta_h^1 \sim \frac{1}{d} N(\mathbf{0}, \mathbf{I})$, networks $\phi_h^1(\cdot, \cdot | \mathbf{W}_h^1)$ (Xu et al., 2022), $Q_h^1 = (\theta_h^1)^\top \phi_h^1(\cdot, \cdot)$, and the target value-networks $\bar{Q}_h^1 = Q_h^1$, where $h \in [H]$
- 3: **for** episode $m = 1$ **to** M **do**
- 4: Sample the initial state of the episode s_1^m
- 5: **for** step $h = 1, 2, \dots, H$ **do**
- 6: Conduct action $a_h^m = \arg \max_a Q_h^m(s_h^m, a)$ and get the next state s_{h+1}^m and reward r_h^m
- 7: Compute the target value $q_h^m = r_h^m + \max_a \bar{Q}_{h+1}^m(s_{h+1}^m, a)$
- 8: Update $\mathbf{A}_h^{m+1} = \mathbf{A}_h^m + \phi_h^m(\phi_h^m)^\top$ and $\mathbf{b}_h^{m+1} = \mathbf{b}_h^m + q_h^m \phi_h^m$
- 9: Update parameter $\theta_h^{m+1} = (\mathbf{A}_h^{m+1})^{-1} \mathbf{b}_h^{m+1}$
- 10: Update the extraction network to $\phi_h^{m+1}(\cdot, \cdot)$ with parameters $\mathbf{W}_h^{m+1} = \mathbf{W}_h^m + \eta \nabla_{\mathbf{W}_h^m} L_h^m$ where

$$L_h^m = \sum_{t=1}^m \left| (\theta_h^{m+1})^\top \phi_h^m(s_h^t, a_h^t | \mathbf{W}_h^m) - r_h^t - \max_a \bar{Q}_{h+1}^m(s_{h+1}^t, a) \right|^2$$

- 11: Obtain UCB-based uncertainty

$$\beta_h^{m+1}(\cdot, \cdot) = \sqrt{(\phi_h^{m+1}(\cdot, \cdot))^\top (\mathbf{A}_h^{m+1})^{-1} \phi_h^{m+1}(\cdot, \cdot)}$$

- 12: Obtain Thompson Sampling-based uncertainty

$$\Delta \theta_h^{m+1} \sim N(0, (\mathbf{A}_h^{m+1})^{-1}) \implies \beta_h^{m+1}(\cdot, \cdot) = (\Delta \theta_h^{m+1})^\top \phi_h^{m+1}(\cdot, \cdot)$$

- 13: Approximate the action-value function

$$Q_h^{m+1}(\cdot, \cdot) = (\theta_h^{m+1})^\top \phi_h^{m+1}(\cdot, \cdot) + \alpha \beta_h^{m+1}(\cdot, \cdot)$$

- 14: **end for**
 - 15: Update the target network $\bar{Q}_h^{m+1}(\cdot, \cdot) = Q_h^{m+1}(\cdot, \cdot)$, $h \in [H]$
 - 16: **end for**
-

C. Proof of Theorem 4.2

In this section, we establish the cumulative regret bound for Algorithm 3. As \mathcal{U} is a straightforward linear transformation of the embeddings, it approximately preserves the theoretical guarantees of UCB- and Thompson Sampling-based exploration strategies. This ensures the rigor of CAE+, thereby upholding the validity of Theorem 4.2.

Before delving into the detailed theory, we first review the notation used in this appendix. Let π^* denote the true optimal policy and π_m represent the policy executed in episode $m \in [M]$. The action-value and state-value functions corresponding to the policies π^* and π_m are represented by Q^* , V^* , and Q^{π_m} , V^{π_m} , respectively. The relationship between the state-value and action-value functions under a specific policy, such as π_m , is given as follows.

$$\begin{aligned} V_h^{\pi_m}(s) &= \max_a Q_h^{\pi_m}(s, a) \\ Q_h^{\pi_m}(s, a) &= r_h(s, a) + \mathbb{E}_{s_{h+1} \sim \mathbb{P}_h(\cdot|s, a)} V_{h+1}^{\pi_m}(s_{h+1}) \end{aligned}$$

In Algorithm 3, the estimated action-value function at step h in episode m is denoted by $Q_h^m(s, a)$, with the corresponding state-value function represented as $V_h^m(s)$. For clarity of presentation, we introduce the following additional notations.

$$(\mathbb{P}_h V_{h+1}^m)(s_h^m, a_h^m) = \mathbb{E}_{s_{h+1}^m \sim \mathbb{P}_h(\cdot|s_h^m, a_h^m)} V_{h+1}^m(s_{h+1}^m). \quad (15)$$

$$\delta_h^m(s_h^m, a_h^m) = r_h^m + (\mathbb{P}_h V_{h+1}^m)(s_h^m, a_h^m) - Q_h^m(s_h^m, a_h^m). \quad (16)$$

$$\zeta_h^m = V_h^m(s_h^m) - V_h^{\pi_m}(s_h^m) + Q_h^m(s_h^m, a_h^m) - Q_h^{\pi_m}(s_h^m, a_h^m). \quad (17)$$

$$\varepsilon_h^m = (\mathbb{P}_h V_{h+1}^m)(s_h^m, a_h^m) - (\mathbb{P}_h V_{h+1}^{\pi_m})(s_h^m, a_h^m) + V_{h+1}^m(s_{h+1}^m) - V_{h+1}^{\pi_m}(s_{h+1}^m). \quad (18)$$

Specifically, $\delta_h^m(s_h^m, a_h^m)$ represents the temporal-difference error for the state-action pair (s_h^m, a_h^m) . The notations ζ_h^m and ε_h^m capture two sources of randomness, *i.e.*, the selection of action $a_h^m \sim \pi_m(\cdot|s_h^m)$ and the generation of the next state $s_{h+1}^m \sim \mathbb{P}_h(\cdot|s_h^m, a_h^m)$ from the environment.

Proof. **Theorem 4.2.**

Based on Lemma D.1, the cumulative regret in Equation 13 can be decomposed into three terms as follows, where $\langle \cdot, \cdot \rangle$ means the inner product of two vectors.

$$\begin{aligned} \text{Reg}_M &= \sum_{m=1}^M Q_1^*(s_1^m, u_1^m) - Q_1^{\pi_m}(s_1^m, a_1^m) \\ &= \sum_{m=1}^M \sum_{h=1}^H [\mathbb{E}_{\pi^*} [\delta_h^m(s_h, a_h) | s_1 = s_1^m] - \delta_h^m(s_h^m, a_h^m)] + \sum_{m=1}^M \sum_{h=1}^H (\zeta_h^m + \varepsilon_h^m) \\ &\quad + \sum_{m=1}^M \sum_{h=1}^H \mathbb{E}_{\pi^*} [\langle Q_h^m(s_h, \cdot), \pi_h^*(\cdot|s_h) - \pi_m(\cdot|s_h) \rangle | s_1 = s_1^m] \end{aligned}$$

According to the definition of π_m , there is Equation 19.

$$\langle Q_h^m(s_h, \cdot), \pi_h^*(\cdot|s_h) - \pi_m(\cdot|s_h) \rangle \leq 0 \quad (19)$$

Consequently, with probability at least $1 - \sigma$ where $\sigma \in (0, 1)$, the cumulative regret can be bounded as follows.

$$\begin{aligned}
 \text{Reg}_M &\leq \sum_{m=1}^M \sum_{h=1}^H [\mathbb{E}_{\pi^*} [\delta_h^m(s_h, a_h) | s_1 = s_1^m] - \delta_h^m(s_h^m, a_h^m)] + \sum_{m=1}^M \sum_{h=1}^H (\zeta_h^m + \varepsilon_h^m) \\
 &\leq \sum_{m=1}^M \sum_{h=1}^H [\mathbb{E}_{\pi^*} [\delta_h^m(s_h, a_h) | s_1 = s_1^m] - \delta_h^m(s_h^m, a_h^m)] + \sqrt{16MH^3 \log \frac{2}{\sigma_1}} \\
 &\leq H \sqrt{2MH \log \frac{2}{\sigma_2}} + C_2 \alpha H \sqrt{Md \cdot \log(1 + \frac{M}{\lambda d})} \\
 &\quad + \frac{C_3 \cdot HL^3 d^{\frac{5}{2}} M \sqrt{\log(\iota + \frac{1}{\sigma_2} + \frac{M|\mathcal{A}|}{\sigma_2})} \|\mathbf{q} - \tilde{\mathbf{q}}\|_{\mathbf{H}^{-1}}}{\iota^{\frac{1}{6}}} + \sqrt{16MH^3 \log \frac{2}{\sigma_1}} \\
 &\leq C_4 H \sqrt{MH \log \frac{2}{\sigma}} + C_2 \alpha H \sqrt{Md \cdot \log(1 + \frac{M}{\lambda d})} + \frac{C_3 \cdot HL^3 d^{\frac{5}{2}} M \sqrt{\log(\iota + \frac{1}{\sigma} + \frac{M|\mathcal{A}|}{\sigma})} \|\mathbf{q} - \tilde{\mathbf{q}}\|_{\mathbf{H}^{-1}}}{\iota^{\frac{1}{6}}}
 \end{aligned} \tag{20}$$

Specifically, the second inequality is based on Lemma D.2, while the third one is based on Lemma D.3. By choosing $\sigma = \max\{\sigma_1, \sigma_2\}$ and $C_4 \geq \sqrt{2} + 4$, we complete the proof. \square

D. Lemmas

Lemma D.1. *Adapted from Lemma 5.1 of Yang et al. (2020): the regret in Equation 13 can be decomposed as Equation 21, where $\langle \cdot, \cdot \rangle$ means the inner product of two vectors.*

$$\begin{aligned}
 \text{Reg}_M &= \sum_{m=1}^M Q_1^*(s_1^m, u_1^m) - Q_1^{\pi^m}(s_1^m, a_1^m) \\
 &= \sum_{m=1}^M V_1^*(s_1^m) - V_1^{\pi^m}(s_1^m) \\
 &= \sum_{m=1}^M \sum_{h=1}^H [\mathbb{E}_{\pi^*} [\delta_h^m(s_h, a_h) | s_1 = s_1^m] - \delta_h^m(s_h^m, a_h^m)] + \sum_{m=1}^M \sum_{h=1}^H (\zeta_h^m + \varepsilon_h^m) \\
 &\quad + \sum_{m=1}^M \sum_{h=1}^H \mathbb{E}_{\pi^*} [\langle Q_h^m(s_h, \cdot), \pi_h^*(\cdot | s_h) - \pi_m(\cdot | s_h) \rangle | s_1 = s_1^m]
 \end{aligned} \tag{21}$$

Lemma D.2. *Adapted from Lemma 5.3 of Yang et al. (2020): with probability at least $1 - \sigma_1$, the second term in Equation 20 can be bounded as follows:*

$$\sum_{m=1}^M \sum_{h=1}^H (\zeta_h^m + \varepsilon_h^m) \leq \sqrt{16MH^3 \log \frac{2}{\sigma_1}} \tag{22}$$

Lemma D.3. *For any $\sigma_2 \in (0, 1)$, assume the width of the action-value network satisfies:*

$$\iota = \text{poly}(L, d, \frac{1}{\sigma_2}, \log \frac{M|\mathcal{A}|}{\sigma_2}) \tag{23}$$

where L is the number of layers in the action-value network, and $\text{poly}(\cdot)$ means a polynomial function depending on the incorporated variables, and let:

$$\alpha = \sqrt{2(d \cdot \log(1 + \frac{M \cdot \log|\mathcal{A}|}{\lambda}) - \log \sigma_2) + \sqrt{\lambda}} \quad (24)$$

$$\eta \leq C_1(\iota \cdot d^2 M^{\frac{1}{2}} L^6 \cdot \log \frac{M|\mathcal{A}|}{\sigma_2})^{-1} \quad (25)$$

then with probability at least $1 - \sigma_2$, the first term in Equation 20 is bounded as:

$$\begin{aligned} & \sum_{m=1}^M \sum_{h=1}^H [\mathbb{E}_{\pi^*} [\delta_h^m(s_h, a_h) | s_1 = s_1^m] - \delta_h^m(s_h^m, a_h^m)] \\ & \leq H \sqrt{2MH \log \frac{2}{\sigma_2}} + C_2 \alpha H \sqrt{Md \cdot \log(1 + \frac{M}{\lambda d})} + \frac{C_3 \cdot HL^3 d^{\frac{5}{2}} M \sqrt{\log(\iota + \frac{1}{\sigma_2} + \frac{M|\mathcal{A}|}{\sigma_2})} \|\mathbf{q} - \tilde{\mathbf{q}}\|_{\mathbf{H}^{-1}}}{\iota^{\frac{1}{6}}} \end{aligned} \quad (26)$$

Proof. According to Yang et al. (2020), there is:

$$\sum_{m=1}^M \sum_{h=1}^H [\mathbb{E}_{\pi^*} [\delta_h^m(s_h, a_h) | s_1 = s_1^m] - \delta_h^m(s_h^m, a_h^m)] \leq \sum_{m=1}^M \sum_{h=1}^H -\delta_h^m(s_h^m, a_h^m) \quad (27)$$

Considering $\delta_h^m(s_h^m, a_h^m)$, it can be decomposed as:

$$\begin{aligned} \delta_h^m(s_h^m, a_h^m) &= r_h^m + (\mathbb{P}_h V_{h+1}^m)(s_h^m, a_h^m) - Q_h^m(s_h^m, a_h^m) \\ &= r_h^m + (\mathbb{P}_h V_{h+1}^m)(s_h^m, a_h^m) - Q_h^*(s_h^m, a_h^m) + Q_h^*(s_h^m, a_h^m) - Q_h^m(s_h^m, a_h^m) \\ &= \mathbb{P}_h(V_{h+1}^m - V_{h+1}^*)(s_h^m, a_h^m) + (Q_h^* - Q_h^m)(s_h^m, a_h^m) \\ &= \underbrace{\mathbb{P}_h(V_{h+1}^m - V_{h+1}^*)(s_h^m, a_h^m)}_{\omega_h^m} - \underbrace{(V_{h+1}^m - V_{h+1}^*)(s_{h+1}^m)}_{\rho_{h+1}^m} + \underbrace{(V_{h+1}^m - V_{h+1}^*)(s_{h+1}^m)}_{\rho_{h+1}^m} + \underbrace{(Q_h^* - Q_h^m)(s_h^m, a_h^m)}_{\varphi_h^m} \end{aligned} \quad (28)$$

By Azuma-Hoeffding inequality, we can bound $\sum_{m=1}^M \sum_{h=1}^H \omega_h^m$ as Equation 29 with probability at least $1 - \sigma_3$.

$$-H \sqrt{2MH \log \frac{2}{\sigma_3}} \leq \sum_{m=1}^M \sum_{h=1}^H \omega_h^m \leq H \sqrt{2MH \log \frac{2}{\sigma_3}} \quad (29)$$

As ρ_{h+1}^m can be decomposed as Equation 30 where $u_{h+1}^m \sim \pi_{h+1}^*(\cdot | s_{h+1}^m)$, there is Equation 31.

$$\rho_{h+1}^m = (V_{h+1}^m - V_{h+1}^*)(s_{h+1}^m) = Q_{h+1}^m(s_{h+1}^m, a_{h+1}^m) - Q_{h+1}^*(s_{h+1}^m, u_{h+1}^m) \quad (30)$$

$$\Rightarrow \sum_{m=1}^M \sum_{h=1}^H (\rho_{h+1}^m + \varphi_h^m) \quad (31)$$

$$\begin{aligned}
 &= \sum_{m=1}^M \sum_{h=1}^{H-1} [Q_{h+1}^m(s_{h+1}^m, a_{h+1}^m) - Q_{h+1}^*(s_{h+1}^m, u_{h+1}^m)] + \sum_{m=1}^M \sum_{h=1}^H (Q_h^* - Q_h^m)(s_h^m, a_h^m) \\
 &= \underbrace{\sum_{m=1}^M \sum_{h=2}^H Q_h^*(s_h^m, a_h^m) - Q_h^*(s_h^m, u_h^m)}_{\text{Reg}_{\text{MAB}}} + \sum_{m=1}^M (Q_1^* - Q_1^m)(s_1^m, a_1^m) \tag{32}
 \end{aligned}$$

Specifically, the second equation is because of $Q_{H+1}^*(s_{H+1}^m, a_{H+1}^m) = 0$ and $Q_{H+1}^m(s_{H+1}^m, a_{H+1}^m) = 0$. The second term in Equation 32 originates from the estimation error of the action-value function, which is constrained by the convergence properties of DQN. Consequently, to complete the proof of Lemma D.3, it suffices to establish a bound for the Reg_{MAB} term, while the second term is omitted for conciseness in the remaining discussion. Bounds of Reg_{MAB} under UCB- and Thompson Sampling-based exploration are proved in Lemma D.7 and Lemma D.8, respectively. Choosing $\sigma_2 = \max\{\sigma_3, \sigma_4\}$ and $C_2 = \max\{C_{ucb}, C_{ts}\}$ completes this proof. \square

D.1. Regret Bound of UCB-based Exploration

In this subsection, we first introduce the standard assumptions in the literature of *deep representation and shallow exploration* in Neural MAB as Assumption D.4, Assumption D.5, and Assumption D.6, which are adapted from Xu et al. (2022).

Assumption D.4. Assume that $\|(s; a)\|_2 = 1$ for $\forall s \in \mathcal{S}, \forall a \in \mathcal{A}$, and that the entries of $(s; a)$ satisfy Equation 33, where D represents the dimension of $(s; a)$. Notably, even if the original state-action pairs do not satisfy this assumption, they can be easily preprocessed to meet it.

$$(s; a)_j = (s; a)_{j+\frac{D}{2}} \tag{33}$$

Assumption D.5. For $\forall s_1, s_2 \in \mathcal{S}$ and $\forall a_1, a_2 \in \mathcal{A}$, there is a constant $l_{Lip} > 0$, such that:

$$\|\nabla_{\mathbf{w}} \phi(s_1, a_1 | \mathbf{W}_h^1) - \nabla_{\mathbf{w}} \phi(s_2, a_2 | \mathbf{W}_h^1)\|_2 \leq l_{Lip} \|(s_1; a_1) - (s_2; a_2)\|_2 \tag{34}$$

Assumption D.6. The neural tangent kernel \mathbf{H} of the action-value network is positive definite.

Lemma D.7. Adapted from Theorem 4.4 of Xu et al. (2022): suppose the standard initializations and assumptions hold. Additionally, assume without loss of generality that $\|\theta^*\|_2 \leq 1$ and $\|\phi(s_h, a_h)\|_2 \leq 1$. If with the UCB-based exploration, then for any $\sigma_4 \in (0, 1)$, let the width of the action-value network satisfies:

$$\iota = \text{poly}\left(L, d, \frac{1}{\sigma_4}, \log \frac{M|\mathcal{A}|}{\sigma_4}\right) \tag{35}$$

where L is the number of layers in the action-value network, and $\text{poly}(\cdot)$ means a polynomial function depending on the incorporated variables, and let:

$$\alpha = \sqrt{2(d \cdot \log(1 + \frac{M \cdot \log|\mathcal{A}|}{\lambda}) - \log \sigma_4)} + \sqrt{\lambda} \tag{36}$$

$$\eta \leq C_1 (\iota \cdot d^2 M^{\frac{11}{2}} L^6 \cdot \log \frac{M|\mathcal{A}|}{\sigma_4})^{-1} \tag{37}$$

then with probability at least $1 - \sigma_4$, the term Reg_{UCB} in Equation 32 can be bounded as follows:

$$\text{Reg}_{\text{UCB}} \leq C_{ucb} \cdot \alpha H \sqrt{Md \cdot \log(1 + \frac{M}{\lambda d})} + \frac{C_3 \cdot HL^3 d^{\frac{5}{2}} M \sqrt{\log(\iota + \frac{1}{\sigma_4} + \frac{M|A|}{\sigma_4})}}{\iota^{\frac{1}{6}}} \|\mathbf{q} - \tilde{\mathbf{q}}\|_{\mathbf{H}^{-1}} \quad (38)$$

where C_1, C_{ucb}, C_3 are constants independent of the problem; $\mathbf{q} = (q_1^1; q_2^1; \dots; q_H^1; \dots; q_H^M)$ and $\tilde{\mathbf{q}} = (Q_1^1(s_1^1, a_1^1); Q_2^1(s_2^1, a_2^1); \dots; Q_H^1(s_H^1, a_H^1); \dots; Q_H^M(s_H^M, a_H^M))$ are the target and the estimated value vectors, respectively.

Notably, the proof of the above lemma relies on the concentration of self-normalized stochastic processes. However, since Q_h^m is not independent of $Q_h^1, Q_h^2, \dots, Q_h^{m-1}$, this result cannot be directly applied. Instead, a similar approach to that in Yang et al. (2020) can be adopted. For simplicity in presentation, we have not explicitly addressed this issue in the proof above, but it is important to bear this limitation in mind.

D.2. Regret Bound of Thompson Sampling-based Exploration

Lemma D.8. *Under the same settings as those of Lemma D.7, if with the Thompson Sampling-based exploration, the term $\text{Reg}_{\text{Thompson Sampling}}$ in Equation 32 can be bounded as Equation 39, where C_{ts} is another problem-independent constant.*

$$\text{Reg}_{\text{Thompson Sampling}} \leq C_{ts} \cdot \alpha H \sqrt{Md \cdot \log(1 + \frac{M}{\lambda d})} + \frac{C_3 \cdot HL^3 d^{\frac{5}{2}} M \sqrt{\log(\iota + \frac{1}{\sigma_4} + \frac{M|A|}{\sigma_4})}}{\iota^{\frac{1}{6}}} \|\mathbf{q} - \tilde{\mathbf{q}}\|_{\mathbf{H}^{-1}} \quad (39)$$

Proof. According to Lemma A.1 of Xu et al. (2022), $Q_h^*(s, u) - Q_h^*(s, a)$ can be decomposed as Equation 40, where $g(s, a; \mathbf{W}) = \nabla_{\mathbf{W}} \phi(s, a; \mathbf{W})$.

$$\begin{aligned} & Q_h^*(s, u) - Q_h^*(s, a) \\ &= (\boldsymbol{\theta}_h^*)^\top [\phi(s, u; \mathbf{W}_h^m) - \phi(s, a; \mathbf{W}_h^m)] + (\boldsymbol{\theta}_h^1)^\top [g(s, u; \mathbf{W}_h^1) - g(s, a; \mathbf{W}_h^1)] (\mathbf{W}_h^* - \mathbf{W}_h^m) \\ &= (\boldsymbol{\theta}_h^1)^\top [g(s, u; \mathbf{W}_h^1) - g(s, a; \mathbf{W}_h^1)] (\mathbf{W}_h^* - \mathbf{W}_h^m) \\ &\quad + \underbrace{(\boldsymbol{\theta}_h^m)^\top [\phi(s, u; \mathbf{W}_h^m) - \phi(s, a; \mathbf{W}_h^m)]}_{\vartheta_h^m} - (\boldsymbol{\theta}_h^m - \boldsymbol{\theta}_h^*)^\top [\phi(s, u; \mathbf{W}_h^m) - \phi(s, a; \mathbf{W}_h^m)] \end{aligned} \quad (40)$$

Based on the action selection process using Thompson Sampling-based exploration in Algorithm 3, we derive Equation 41.

$$(\boldsymbol{\theta}_h^m + \alpha_h^m \Delta \boldsymbol{\theta}_h^m)^\top \phi(s, u; \mathbf{W}_h^m) \leq (\boldsymbol{\theta}_h^m + \alpha_h^m \Delta \boldsymbol{\theta}_h^m)^\top \phi(s, a; \mathbf{W}_h^m) \quad (41)$$

Consequently, ϑ_h^m can be bounded as Equation 42.

$$\begin{aligned} \vartheta_h^m &\leq \|\Delta \boldsymbol{\theta}_h^m\|_{\mathbf{A}_h^m} \|\phi(s, a; \mathbf{W}_h^m) - \phi(s, u; \mathbf{W}_h^m)\|_{(\mathbf{A}_h^m)^{-1}} \\ &\leq (\sqrt{d} + \sqrt{2 \log \frac{1}{\sigma_4}}) \|\phi(s, a; \mathbf{W}_h^m) - \phi(s, u; \mathbf{W}_h^m)\|_{(\mathbf{A}_h^m)^{-1}} \end{aligned} \quad (42)$$

Specifically, the last inequality above is because $\Delta \boldsymbol{\theta}_h^m \sim N(0, (\mathbf{A}_h^m)^{-1})$. Substituting the bound of ϑ_h^m back into Equation 40 further yields:

$$Q_h^*(s, u) - Q_h^*(s, a) \leq (\boldsymbol{\theta}_h^1)^\top [g(s, u; \mathbf{W}_h^1) - g(s, a; \mathbf{W}_h^1)] (\mathbf{W}_h^* - \mathbf{W}_h^m) \quad (43)$$

$$\begin{aligned}
 & + (\sqrt{d} + \sqrt{2 \log \frac{1}{\sigma_4}}) \|\phi(s, a; \mathbf{W}_h^m) - \phi(s, u; \mathbf{W}_h^m)\|_{(\mathcal{A}_h^m)^{-1}} \\
 & - (\boldsymbol{\theta}_h^m - \boldsymbol{\theta}_h^*)^\top [\phi(s, u; \mathbf{W}_h^m) - \phi(s, a; \mathbf{W}_h^m)]
 \end{aligned}$$

Comparing Equation 43 with A.7 of Xu et al. (2022), the difference between the regrets of Thompson Sampling-based and UCB-based exploration is bounded as Equation 44, with probability at least $1 - \sigma_4$.

$$\begin{aligned}
 & \left| \text{Reg}_{\text{Thompson Sampling}} - \text{Reg}_{\text{UCB}} \right| \\
 & \leq \sum_{m=1}^M \sum_{h=1}^H (\sqrt{d} + \sqrt{2 \log \frac{1}{\sigma_4}}) \|\phi(s, a; \mathbf{W}_h^m) - \phi(s, u; \mathbf{W}_h^m)\|_{(\mathcal{A}_h^m)^{-1}} \\
 & \quad + \sum_{m=1}^M \sum_{h=1}^H \alpha_h^m \|\phi(s, a; \mathbf{W}_h^m)\|_{(\mathcal{A}_h^m)^{-1}} + \sum_{m=1}^M \sum_{h=1}^H \alpha_h^m \|\phi(s, u; \mathbf{W}_h^m)\|_{(\mathcal{A}_h^m)^{-1}} \\
 & \leq H \sqrt{Md \log(1 + \frac{M}{\lambda d})} (\sqrt{d \log(1 + \frac{M \log MA}{\lambda})} + \log \frac{1}{\sigma_4} + \sqrt{\lambda}) \\
 & \leq C_5 \alpha H \sqrt{Md \cdot \log(1 + \frac{M}{\lambda d})} \tag{44}
 \end{aligned}$$

Setting $C_{ts} = C_{ucb} + C_5$ completes the proof. \square

Specifically, the second inequality above is based on the concentration of self-normalized stochastic processes. Similarly to the proof of UCB-based exploration, since Q_h^m is not independent of $Q_h^1, Q_h^2, \dots, Q_h^{m-1}$, it cannot be directly applied. However, we can alternatively adopt a similar approach to that in Yang et al. (2020), which we do not discuss more here.

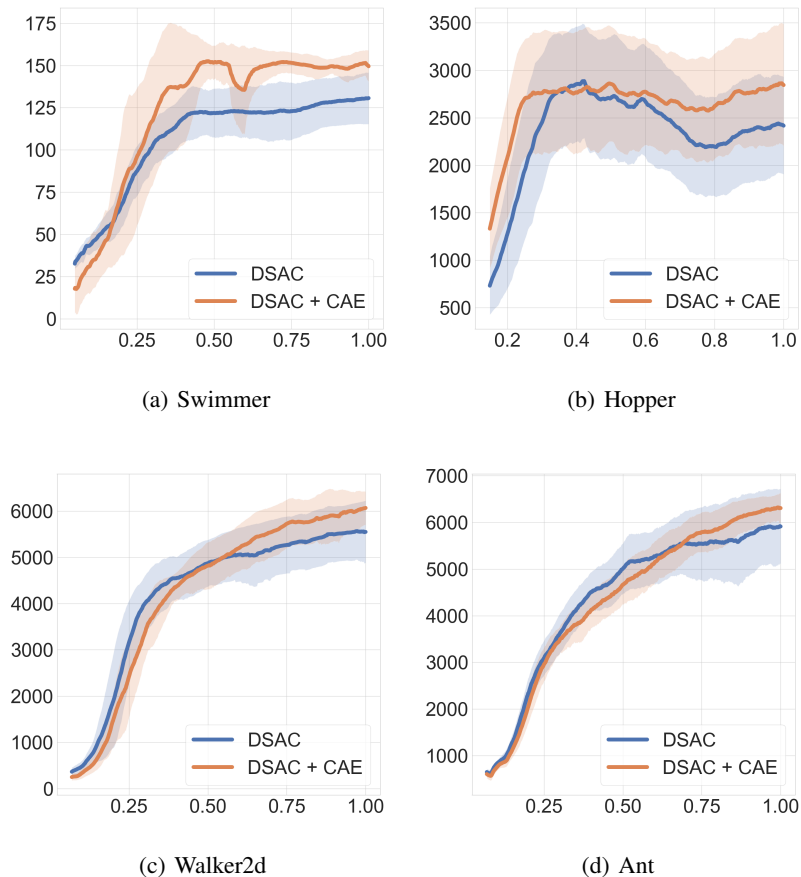


Figure 5. Experimental results on MuJoCo-v3.

E. Experiment

In this section, we present the hyperparameters used to replicate the experimental results discussed in this paper and additional experimental results, respectively, for the MuJoCo and MiniHack tasks.

E.1. Experiment on Mujoco

Table 6. Exploration coefficient for various MuJoCo tasks and algorithms

Env	Algorithms			
	SAC	PPO	TD3	DSAC
Swimmer	0.2	0.1	0.1	0.1
Ant	0.7	0.2	0.3	1.0
Walker2d	1.0	0.13	0.8	3.0
Hopper	0.4	0.14	0.3	2.0
HalfCheetah	0.4	0.5	3.7	3.0
Humanoid	4.0	0.1	6.0	4.5

Hyperparameters of various algorithms for the experiments on MuJoCo are completely the same as those in the public codebase CleanRL. CAE introduces only two more hyperparameters, *i.e.*, the exploration coefficient α and the ridge which is

set as $\lambda = 1$. The exploration coefficients are summarized in Table 6 for various tasks and algorithms, and the experimental results on various MuJoCo tasks involving different RL algorithms are in Figure 5 and Figure 6. Notably, we only present results for cases where the *RPI* exceeds 5.0%, as smaller *RPI* values are not clearly distinguishable in the figures.

E.2. Experiment on MiniHack

The hyperparameters for IMPALA, E3B, CAE, and CAE+ used in our experiments are summarized in Table 7 and Table 8, aligning with those from the E3B experiments (Henaff et al., 2022). The experimental results on MiniHack are presented in Figure 7. Notably, CAE+ outperforms E3B across all sixteen tasks evaluated in Henaff et al. (2022). For clarity and conciseness, we report results for a representative subset of these tasks.

Table 7. IMPALA Hyperparameters for MiniHack (Henaff et al., 2022)

Learning rate	0.0001
RMSProp smoothing constant	0.99
RMSProp momentum	0
RMSProp	10^{-5}
Unroll length	80
Number of buffers	80
Number of learner threads	4
Number of actor threads	8
Max gradient norm	40
Entropy cost	0.0005
Baseline cost	0.5
Discounting factor	0.99

Table 8. E3B and CAE+ Hyperparameters for MiniHack

E3B and CAE+	Running intrinsic reward normalization	true
	Ridge regularizer	0.1
	Entropy Cost	0.005
	Exploration coefficient	1
CAE+	Dimension of U	256

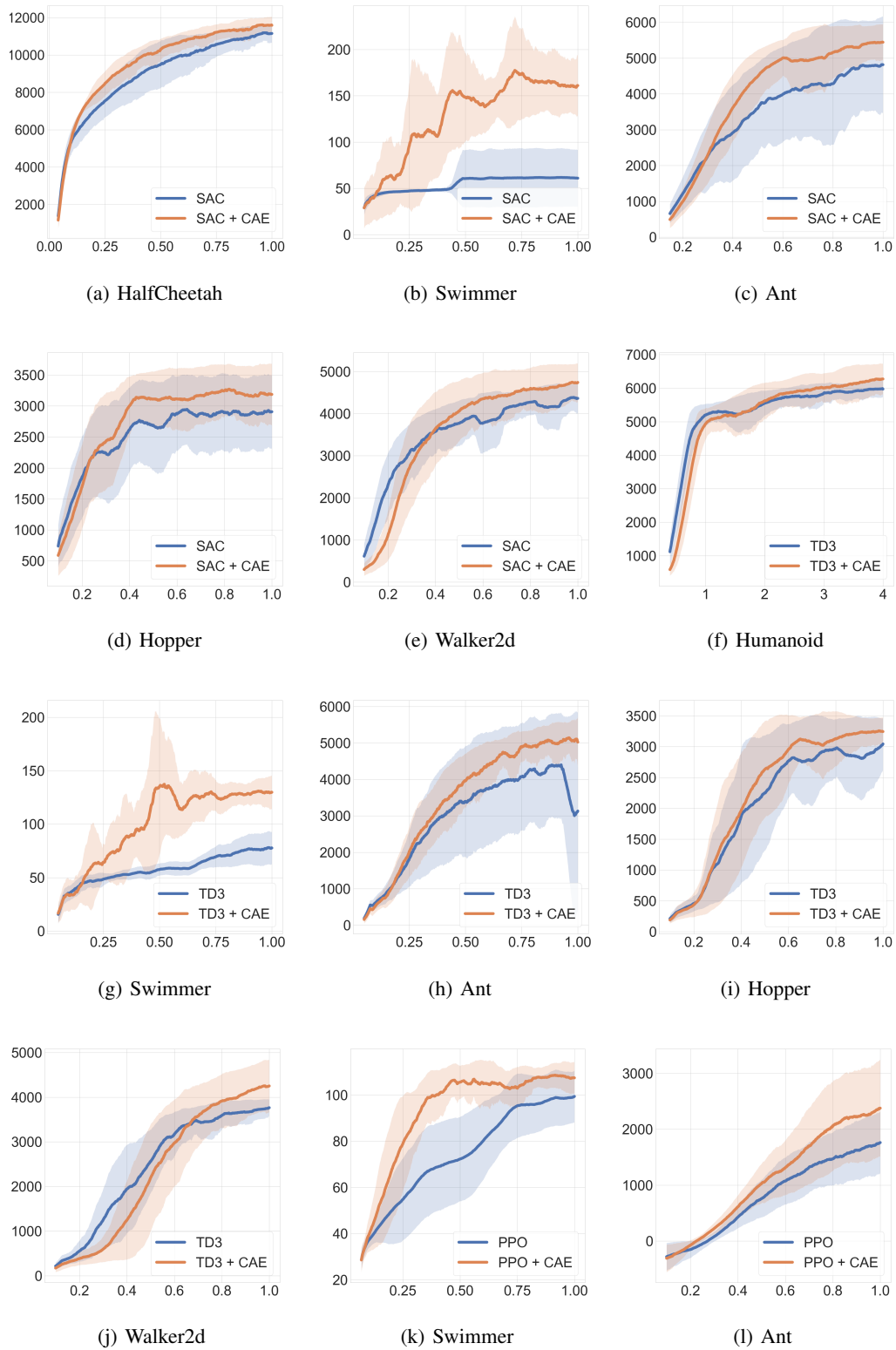


Figure 6. Experimental results on MuJoCo-v4.

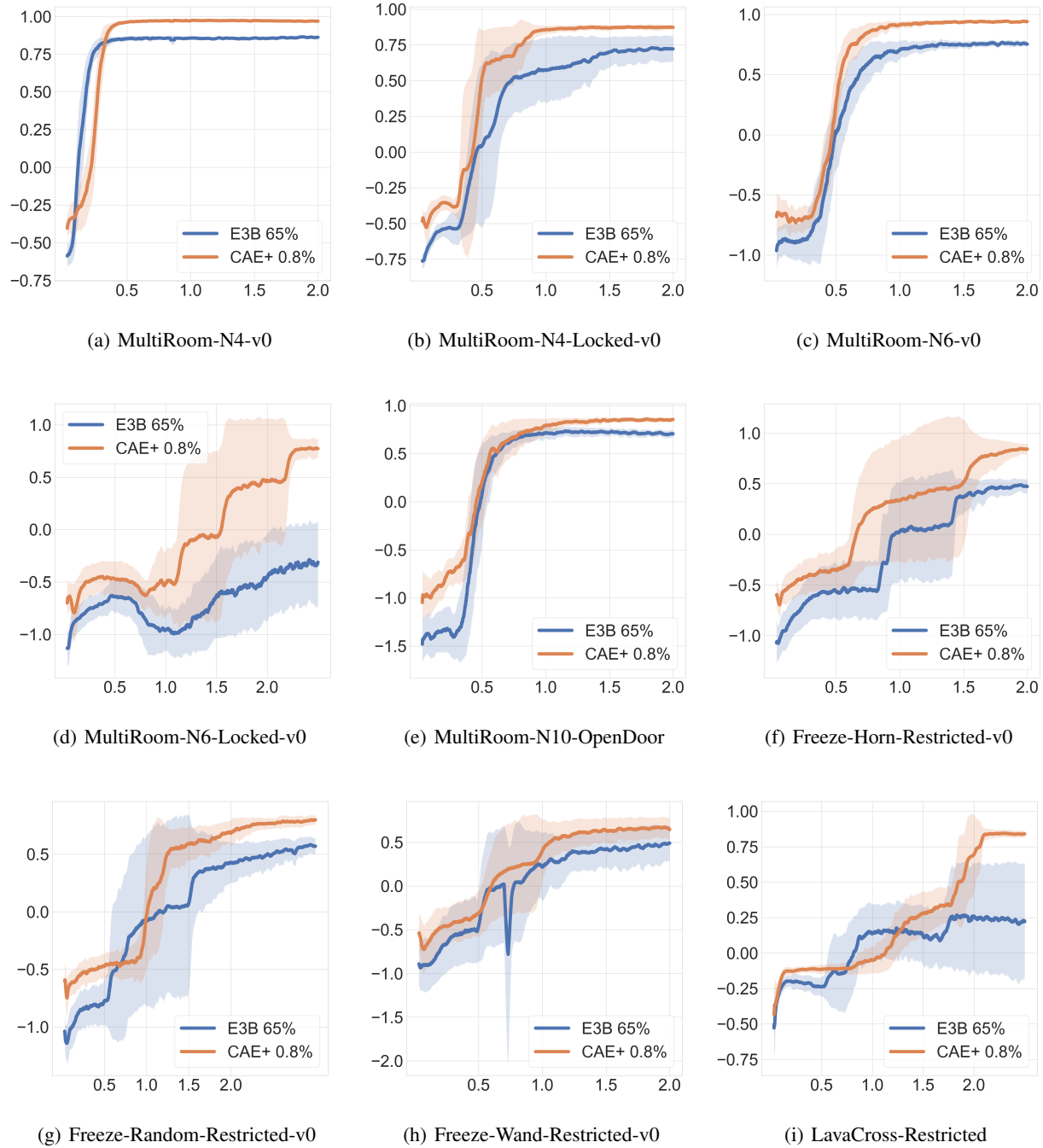


Figure 7. Experimental results on MiniHack.